Geophysical Journal International

Geophys. J. Int. (2017) **211,** 663–672
Advance Access publication 2017 July 22
GJI Marine geosciences and applied geophysics

doi: 10.1093/gji/ggx293

Incorporating sediment compaction into a gravitationally self-consistent model for ice age sea-level change

Ken L. Ferrier,[1] Jacqueline Austermann,[2] Jerry X. Mitrovica[3] and Tamara Pico[3]

[1] *Georgia Institute of Technology, School of Earth and Atmospheric Sciences, Atlanta, GA* 30332-0340, *USA. E-mail: ferrier@gatech.edu*
[2] *Department of Earth Sciences, University of Cambridge, Cambridge CB*2 3*EQ, United Kingdom*
[3] *Department of Earth and Planetary Sciences, Harvard University, Cambridge, MA* 02138, *USA*

Accepted 2017 July 11. Received 2017 July 6; in original form 2016 November 4

SUMMARY

Sea-level changes are of wide interest because they regulate coastal hazards, shape the sedimentary geologic record and are sensitive to climate change. In areas where rivers deliver sediment to marine deltas and fans, sea-level changes are strongly modulated by the deposition and compaction of marine sediment. Deposition affects sea level by increasing the elevation of the seafloor, by perturbing crustal elevation and gravity fields and by reducing the volume of seawater through the incorporation of water into sedimentary pore space. In a similar manner, compaction affects sea level by lowering the elevation of the seafloor and by purging water out of sediments and into the ocean. Here we incorporate the effects of sediment compaction into a gravitationally self-consistent global sea-level model by extending the approach of Dalca *et al.* (2013). We show that incorporating compaction requires accounting for two quantities that are not included in the Dalca *et al.* (2013) analysis: the mean porosity of the sediment and the degree of saturation in the sediment. We demonstrate the effects of compaction by modelling sea-level responses to two simplified 122-kyr sediment transfer scenarios for the Amazon River system, one including compaction and one neglecting compaction. These simulations show that the largest effect of compaction is on the thickness of the compacting sediment, an effect that is largest where deposition rates are fastest. Compaction can also produce minor sea-level changes in coastal regions by influencing shoreline migration and the location of seawater loading, which perturbs crustal elevations. By providing a tool for modelling gravitationally self-consistent sea-level responses to sediment compaction, this work offers an improved approach for interpreting the drivers of past sea-level changes.

Key words: Geomorphology; Sea level change; Sedimentary basin processes.

1 INTRODUCTION

Sea level varies over a wide range of timescales and is of interest in a number of Earth science disciplines. Over million-year timescales, changes in sea level influence sedimentary and geomorphic processes, which motivate efforts to infer palaeoclimatic information from sedimentary sequences and marine terraces (e.g. Chappell 1974). Over millennial timescales, changes in sea level alter the connectivity between neighbouring landmasses, shaping the migratory history of humans and other species (e.g. d'Alpoim Guedes *et al.* 2016). Over the coming decades, sea level is expected to change rapidly, with global mean sea level projected to be 19 to 83 cm higher in 2100 than it was in 1985–2005 (Church *et al.* 2013). Coastal flooding and erosion hazards associated with the projected sea-level rise spur ongoing efforts to better understand the drivers of sea-level change.

The hazards associated with rapid sea-level change can be accentuated in places where rivers deliver sediment to deltas and fans, because sea-level changes in these areas are strongly modulated by the deposition and compaction of sediment (e.g. Wolstencroft *et al.* 2014; Ferrier *et al.* 2015). Deposition affects sea level by increasing the elevation of the seafloor, by perturbing crustal elevation and gravity fields and by reducing the volume of ocean water through the incorporation of water into sedimentary pore space. Similarly, compaction affects sea level by lowering the elevation of the seafloor and by purging water out of sediments and into the ocean. These effects can be large. In rivers with large sediment fluxes like the Ganges-Brahmaputra, deposition rates on the subaqueous delta range from 10 to 60 mm yr^{-1} and coastal subsidence rates can exceed 5 mm yr^{-1} (Kuehl *et al.* 1997; Michels *et al.* 2003; Khan & Islam 2008; Wilson & Goodbred 2014). Such rates are large in the context of global mean sea level changes that averaged 1.2 ± 0.2 mm yr^{-1} over 1901–1990 and accelerated to 3.0 ± 0.7 mm yr^{-1} from 1993 to 2010 (Hay *et al.* 2015). Field observations elsewhere show that compaction can significantly affect the elevation of palaeo-sea-level markers over millennial timescales at many sites, including the US

Atlantic coast (e.g. Bloom 1964; Kaye & Barghoorn 1964; Horton *et al.* 2013; Brain *et al.* 2015), the Gulf of Mexico (e.g. Törnqvist *et al.* 2008), Great Britain (e.g. Edwards 2006; Horton & Shennan 2009; Brain *et al.* 2012), Italy (e.g. Teatini *et al.* 2011) and the Yellow Sea (Pico *et al.* 2016). These studies highlight the importance of accounting for compaction in interpretations of past sea-level change and forecasts of future sea-level change (e.g. Blum & Roberts 2009).

To date, sediment compaction has not been incorporated into theories of gravitationally self-consistent sea-level change. Since Farrell & Clark (1976) introduced the classic treatment of gravitationally self-consistent sea level change, sea-level models have built upon this framework to include the effects of Earth rotation (e.g. Milne & Mitrovica 1996, 1998), three-dimensional Earth structure (e.g. Martinec 2000; Wu & van der Wal 2003; Zhong *et al.* 2003; Latychev *et al.* 2005), shoreline migration (Johnston 1993; Peltier 1994; Milne 1998; Milne *et al.* 1999), changes in the extent of grounded marine-based ice (Milne 1998; Peltier 1998; Milne *et al.* 1999; Lambeck *et al.* 2003; Kendall *et al.* 2005), sediment erosion and deposition (Dalca *et al.* 2013) and dynamic topography (Austermann & Mitrovica 2015). Among these studies, Dalca *et al.* (2013) was the first to incorporate sediment transfer, but that study did not account for sea-level changes that result from the gradual compaction of sediment after deposition. The absence of a gravitationally self-consistent model that includes the effects of sediment compaction presents a gap in our ability to model sea-level changes in areas affected by sediment.

Here we show how to close that gap. Our goal is to explore how the compaction of sediment generates changes in sea level within a gravitationally self-consistent sea-level model. We begin by reviewing the mathematical framework for sea-level change in Dalca *et al.* (2013) and demonstrate how to extend it to account for sediment compaction. We then adopt a parametrization for sediment compaction and illustrate its behaviour by applying it to a 1-D column of saturated sediment. We incorporate this parametrization for compaction into the global sea-level model and apply it to two simplified scenarios for sediment erosion and deposition in the Amazon basin and offshore fan, one including compaction and the other neglecting compaction. While compaction happens fastest shortly after deposition, our analyses show that compaction can significantly affect sea-level changes over $\sim 10^5$ yr timescales, which highlights the importance of accounting for compaction over glacial-interglacial timescales.

2 A GRAVITATIONALLY SELF-CONSISTENT FRAMEWORK FOR GLOBAL SEA-LEVEL RESPONSES TO SEDIMENT COMPACTION

In classic treatments of post-glacial sea-level change, sea level is defined as the elevation difference between the sea-surface equipotential G and the solid surface, which is defined as the sum of the elevation of the crust R, the grounded ice thickness I and the sediment thickness H (Farrell & Clark 1976; Dalca *et al.* 2013; Fig. 1),

$$SL = G - R - I - H. \tag{1}$$

Each term in eq. (1), including SL, is defined globally and is a function of time. Changes in sea level ΔSL from one time t_0 to a later time t_j are similarly globally defined, and are given by the

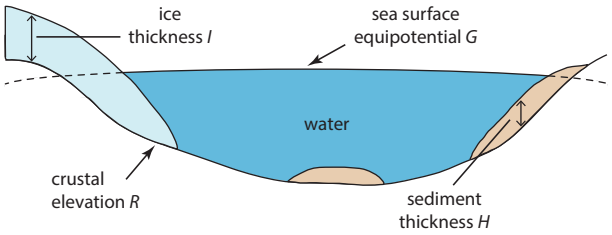

Figure 1. Schematic illustration of the terms in the sea-level equation (eq. 2).

so-called sea-level equation (eq. 2; Farrell & Clark 1976; Dalca *et al.* 2013),

$$\Delta SL = \Delta G - \Delta R - \Delta I - \Delta H. \tag{2}$$

Here ΔG is the change in the sea surface elevation from t_0 to t_j, ΔR is the change in the elevation of the crust, ΔI is the change in the thickness of grounded ice and ΔH is the change in the thickness of sediment. The inclusion of ΔH in eq. (2) is necessary because sediment directly affects the elevation of the solid surface, and it is useful because it permits the computation of sea-level responses to changes in sediment loading (Dalca *et al.* 2013).

Marine sediment deposition and compaction generates changes in sea level in a few ways. First, deposition affects sea level by increasing ΔH, which increases the elevation of the seafloor and thereby decreases ΔSL in eq. (2). During deposition, seawater is incorporated into the sedimentary pore space, which reduces the volume of seawater. In a similar manner, compaction of submarine sediment affects sea level by lowering the elevation of the seafloor and purging water out of the sedimentary pore space, which increases the volume of seawater. The redistribution of sediment also produces changes in the gravity field that generate changes in sea level, an effect that is fully captured by gravitationally self-consistent sea-level models (Dalca *et al.* 2013; Wolstencroft *et al.* 2014; Ferrier *et al.* 2015). This framework also captures the effects of sediment redistribution on ocean basin geometry, because changes in ocean basin geometry are entirely determined by changes in the solid surface elevation (ΔH and ΔR) and the sea surface elevation (ΔG). The main goal of this study is to show how deposition and compaction induce changes in sea level via these processes within a gravitationally self-consistent framework for global sea-level change.

We begin by considering a column of porous sediment of thickness H (Fig. 2). The sediment column consists of sediment grains of density ρ_s and pore space between the grains that may be filled with water or air. The bulk density of the sediment at a depth z below the upper surface of the sediment column, $\rho_H(z)$, depends on the porosity, $\phi(z)$, and the density of the fluid filling the pore space, $\rho_{\text{pore fluid}}$:

$$\rho_H(z) = \rho_s - (\rho_s - \rho_{\text{pore fluid}})\phi(z), \quad \text{for} \quad z > 0. \tag{3}$$

In the case of saturated sediment like that in a submarine delta, the pores are filled with water and the bulk density is $\rho_H(z) = \rho_s - (\rho_s - \rho_w)\phi(z)$, where ρ_w is the density of water. In the case of dry sediment, like that in a dry alluvial fan, the pores are filled with air, which has a density over 1000 times smaller than ρ_s, and the bulk density is well approximated as $\rho_H(z) \approx \rho_s(1 - \phi(z))$.

Defining the degree of saturation f_w as the fraction of a sediment column's total pore space that is filled with water, the mean bulk density of the sediment column, $\bar{\rho}_H$, can be written as a function of the mean porosity of the sediment column, $\bar{\phi}$:

$$\bar{\rho}_H = \rho_s - (\rho_s - \rho_w f_w)\bar{\phi} \tag{4}$$

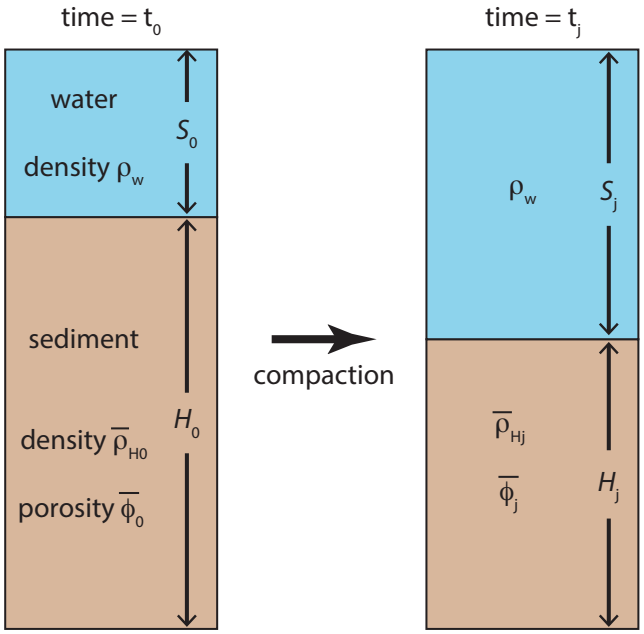

Figure 2. Sediment compaction between times t_0 and t_j induces changes in sediment thickness (H_0 to H_j), mean sediment density ($\bar{\rho}_{H0}$ to $\bar{\rho}_{Hj}$), mean sediment porosity ($\bar{\phi}_0$ to $\bar{\phi}_j$) and the thickness of the overlying water column (S_0 to S_j).

Like the terms in eq. (1), each of the terms in eq. (4) is a globally defined scalar field that can vary in space and time. For simplicity in this study, we assume water density ρ_w and sediment grain density ρ_s are each constant in space and time.

2.1 Effects of sediment compaction and deposition on the load

Incorporating sediment compaction requires accounting for changes in the sediment and water loads. In practice, this requires modifying four equations that account for changes in the sediment and water loads and the elevation of the sea-surface equipotential in the sea-level model of Dalca *et al.* (2013). The first describes the load on the crust due to the overlying masses of water, ice and sediment. Dalca *et al.* (2013) wrote the load as $L = \rho_w S + \rho_I I + \rho_H H$, where ρ_w, ρ_I and ρ_H are the densities of seawater, ice and sediment, respectively, and S, I and H are the thicknesses of seawater, ice and sediment, respectively. This equation implicitly assumes that sediments maintain a constant density over time, and thus neglects sediment compaction. To account for sediment compaction, we use eq. (4) to rewrite the load as

$$\begin{aligned} L &= \rho_w S + \rho_I I + \bar{\rho}_H H \\ &= \rho_w S + \rho_I I + [\rho_s - (\rho_s - \rho_w f_w)\bar{\phi}]H. \end{aligned} \tag{5}$$

For simplicity, eq. (5) takes the density of the pore water in the sediment to be the same as the density of the overlying seawater, thereby neglecting changes in pore fluid density that can occur during diagenesis. This equation for the load differs from that in Dalca *et al.* (2013) in that it permits the mean sediment density to change over time through changes in the mean porosity and the fraction of the pore space filled with water.

The second equation in Dalca *et al.* (2013) that requires modification describes the change in the load ΔL_j from time t_0 to time t_j, which Dalca *et al.* wrote as $\Delta L_j = \rho_w \Delta S_j + \rho_I \Delta I_j + \rho_s \Delta H_j$. We use eq. (5) to rewrite this as in eq. (6).

$$\begin{aligned} \Delta L_j &= L_j - L_0 \\ &= \rho_w \Delta S_j + \rho_I \Delta I_j + \left[\rho_s - (\rho_s - \rho_w f_{wj})\bar{\phi}_j\right] H_j \\ &\quad - [\rho_s - (\rho_s - \rho_w f_{w0})\bar{\phi}_0]H_0. \end{aligned} \tag{6}$$

Here the subscript j indicates a quantity's value at time t_j, and the subscript 0 indicates the quantity's value at time t_0. For example, f_{wj} is the degree of saturation at time t_j, and f_{w0} is the degree of saturation at time t_0.

2.2 Effects of sediment compaction and deposition on seawater volume and the gravity field

The third and fourth equations in Dalca *et al.* (2013) that require modification relate to conservation of water mass and its effect on the sea-surface equipotential. As saturated sediment compacts, water squeezes out of the sedimentary pore space and returns to the ocean. This increases the global volume of seawater. Marine sediment deposition does the reverse, incorporating water into sedimentary pore space and decreasing the global volume of seawater. Both deposition and compaction change sea level by changing the height of the sediment-water interface.

In the absence of lateral water transport, compaction induces no changes in the load and hence no load-induced changes in the crustal elevation or the elevation of the sea-surface equipotential. This is the case for compacting submarine sediment (Fig. 2). A counterexample is saturated sediment in continental settings, which, when it compacts, releases water that travels to the ocean through channel networks, thereby changing the spatial distribution of the water load. We do not explore the effects of continental groundwater storage on sea level in this study, but we note that the framework presented here is able to account for this process, and therefore can be used to explore such effects in future studies.

Here we modify the equations that describe the global conservation of water mass to account for sediment compaction and deposition. This treatment assumes that the densities of water and the solid sediment particles remain constant over time, and so neglects diagenetic processes that incorporate water into minerals within the sediment column.

In previous studies of glacial isostatic adjustment, including Dalca *et al.* (2013), conservation of the surface water mass load is expressed as a balance between globally integrated changes in ice and seawater masses. Here we extend this expression to account for water storage in sediment, which is represented by the last term on the right-hand side of the following equation:

$$\iint_\Omega \Delta S_j \mathrm{d}\Omega = -\frac{\rho_I}{\rho_w} \iint_\Omega \Delta I_j \mathrm{d}\Omega - \iint_\Omega (\bar{\phi}_j f_{wj} H_j - \bar{\phi}_0 f_{w0} H_0)\mathrm{d}\Omega \tag{7}$$

The double integral over Ω represents the integral over the Earth's surface. Because the global water budget can affect the elevation of the sea-surface equipotential, this revised expression modifies the equation in Dalca *et al.* (2013) for the spatially uniform change in the elevation of the sea-surface equipotential, $\Delta\Phi_j/\mathrm{g}$.

$$\begin{aligned} \frac{\Delta\Phi_j}{g} &= \frac{-\rho_I}{\rho_w A_j} \iint_\Omega \Delta I_j \mathrm{d}\Omega - \frac{1}{A_j} \iint_\Omega (\bar{\phi}_j f_{wj} H_j - \bar{\phi}_0 f_{w0} H_0)\mathrm{d}\Omega \\ &\quad - \frac{1}{A_j} \iint_\Omega \Delta\mathcal{S}\mathcal{L}_j C_j \mathrm{d}\Omega + \frac{1}{A_j} \iint_\Omega T_0 (C_j - C_0)\mathrm{d}\Omega \end{aligned} \tag{8}$$

Here C is the so-called ocean function, defined as $C = 1$ if $SL > 0$ and $C = 0$ if $SL \leq 0$ (Munk & Macdonald 1960), $A_j = \iint_\Omega C_j \mathrm{d}\Omega$ is the area of the oceans at t_j, $\Delta\mathcal{SL}_j$ is the spatially variable component of the sea-level change at t_j, and T_0 is the topography at t_0.

To summarize, the compaction of sediment can be incorporated into the Dalca *et al.* (2013) sea-level theory by replacing their eqs (6), (17), (27) and (28) with eqs (5)–(8). Inspection of eqs (5)–(8) indicates that incorporating sediment compaction into the gravitationally self-consistent sea-level model requires only two additional quantities that were not accounted for in Dalca *et al.* (2013): the mean porosity, $\bar{\phi}(t)$, and the degree of saturation, $f_w(t)$, in the sedimentary column. An advantage of this framework for including the effects of compaction on sea-level change is its flexibility with respect to the choice of compaction model. That is, the framework permits the use of any model for sediment compaction, as long as the model yields values of $\bar{\phi}(t)$, $f_w(t)$ and $H(t)$ to input into the sea-level model.

2.3 Expressions governing sea-level change under a simplifying assumption about saturation

By considering the degree of saturation f_w, eqs (5)–(8) permit exploration of the full range of possible degrees of saturation in sediment between fully dry and fully saturated. In this study, for the sake of simplicity, we will apply the following rule for saturation: sediment will be fully saturated if it is submarine (i.e. $f_w = 1$ if $SL > 0$) and fully dry if it is subaerial (i.e. $f_w = 0$ if $SL \leq 0$). In this case, the mean bulk density of the sediment column is given by

$$\bar{\rho}_H = \rho_s - (\rho_s - \rho_w C)\bar{\phi}. \tag{9}$$

Similarly, the total load and the change in the total load are given by

$$L = \rho_w S + \rho_I I + [\rho_s - (\rho_s - \rho_w C)\bar{\phi}]H \tag{10}$$

$$\begin{aligned}\Delta L_j = {} & \rho_w \Delta S_j + \rho_I \Delta I_j + [\rho_s - (\rho_s - \rho_w C_j)\bar{\phi}_j]H_j \\ & - [\rho_s - (\rho_s - \rho_w C_0)\bar{\phi}_0]H_0.\end{aligned} \tag{11}$$

Furthermore, the change in the water load is

$$\iint_\Omega \Delta S_j \mathrm{d}\Omega = -\frac{\rho_I}{\rho_w} \iint_\Omega \Delta I_j \mathrm{d}\Omega - \iint_\Omega (\bar{\phi}_j C_j H_j - \bar{\phi}_0 C_0 H_0)\mathrm{d}\Omega, \tag{12}$$

and the spatially invariant change in the elevation of the sea-surface equipotential elevation is computed from

$$\begin{aligned}\frac{\Delta\Phi_j}{g} = {} & \frac{-\rho_I}{\rho_w A_j} \iint_\Omega \Delta I_j \mathrm{d}\Omega - \frac{1}{A_j} \iint_\Omega (\bar{\phi}_j C_j H_j - \bar{\phi}_0 C_0 H_0)\mathrm{d}\Omega \\ & - \frac{1}{A_j} \iint_\Omega \Delta\mathcal{SL}_j C_j \mathrm{d}\Omega + \frac{1}{A_j} \iint_\Omega T_0 (C_j - C_0)\mathrm{d}\Omega\end{aligned} \tag{13}$$

In the numerical results below, we adopt eqs (9)–(13) to illustrate how compaction affects changes in sea level. These equations neglect variations in the degree of saturation in terrestrial sediment, which varies geographically (e.g. Bindlish *et al.* 2015) and over time. Because the only information required about the sediment in this framework is its thickness, density and porosity, the sea-level model can be applied equally well to clastic or organic-rich facies.

It is worth noting how modelled sea-level changes should be compared to field observations of relative sea level (*RSL*), which mark the difference between sea level at a past time t and the present ($RSL(t) = \Delta SL(t) - \Delta SL(0)$). Many *RSL* observations are benchmarked to surfaces untouched by sediment. For example, modern *RSL* observations are commonly measured with tide gauges, whose elevations are benchmarked to bedrock. In such cases, *RSL* observations should be compared to modelled sea-level changes based on ΔG and ΔR alone, rather than from ΔG and ΔR and ΔH. Ferrier *et al.* (2015) showed that this calculation can be performed by computing ΔG and ΔR under the applied sediment load and then setting $\Delta H = 0$ in eq. (2), and denoted the resulting estimate of the sea-level change as $\Delta SL_{\mathrm{GR}} = \Delta G - \Delta R$. For comparison to RSL observations like these, modelled *RSL* should be calculated as $RSL(t) = \Delta SL_{\mathrm{GR}}(t) - \Delta SL_{\mathrm{GR}}(0)$. Other types of palaeo-sea-level observations are benchmarked to palaeo-sea-level markers in compressible sediment, such as dated sedimentary strata that mark the boundary between submarine and subaerial sediment at a given time (e.g. Hanebuth *et al.* 2006; Simms *et al.* 2009; Pico *et al.* 2016). For studies like these, which aim to measure changes in the sea surface elevation relative to a palaeo-sea-level marker (rather than relative to the solid surface, as in eq. 2), comparing modelled sea-level changes to field observations requires properly accounting for compaction under the marker and deposition above the marker. As an example, consider a marker whose elevation is affected by compaction of the underlying sediment by an amount ΔH_{c} from the time of its formation to the present. If additional sediment of thickness ΔH_{d} is deposited atop the marker over the same time, then the total change in sediment thickness over this interval is $\Delta H = \Delta H_{\mathrm{d}} - \Delta H_{\mathrm{c}}$. Compaction of the underlying sediment is directly incorporated into the modelled sea-level change as $\Delta SL = \Delta G - \Delta R - \Delta I - (\Delta H_{\mathrm{d}} - \Delta H_{\mathrm{c}})$ (eq. 2). The resulting change in the sea surface elevation relative to the sea-level marker can then be related to the modelled sea-level change as $\Delta SL_{\mathrm{marker}} = \Delta SL + \Delta H_{\mathrm{d}}$, from which it follows that *RSL* for the sea-level marker can be related to the modelled *RSL* as $RSL_{\mathrm{marker}}(t) = \Delta SL_{\mathrm{marker}}(t) - \Delta SL_{\mathrm{marker}}(0) = RSL(t) - \Delta H_{\mathrm{d}}$.

3 EFFECTS OF COMPACTION ON A 1-D SEDIMENT COLUMN

Solving eqs (9)–(13) requires that the mean porosity in the sediment column over time be computed. To illustrate the effects of sediment compaction on modelled changes in sediment thickness (and hence sea level), we present a thought experiment in which a 1-D sediment column undergoes simultaneous deposition and compaction. Volume conservation dictates that the sediment column grows as sediment is deposited at a rate B, and shrinks as it compacts at a rate F

$$\frac{\mathrm{d}H}{\mathrm{d}t} = B - F. \tag{14}$$

Because the mass per unit area of solid grains in the sediment column, $\rho_s(1 - \bar{\phi})H$, remains constant during compaction, F can be written in terms of the mean porosity

$$F = -\frac{H}{1 - \bar{\phi}} \frac{\mathrm{d}\bar{\phi}}{\mathrm{d}t}. \tag{15}$$

Eq. (15) indicates that calculating the evolution of sediment thickness with eq. (14) requires a parametrization for the rate of change of the mean porosity. Since porosity changes at different rates at different depths within the sedimentary column, this requirement involves tracking changes in the vertical porosity profile over time. A number of models have been proposed for the evolution of porosity profiles and the compaction of sediment under its own weight (e.g. Biot 1941; Gibson *et al.* 1967, 1981; Audet & Fowler 1992;

Pizzuto & Schwendt 1997; Paul & Barras 1998; Villa 2010; Brain *et al.* 2012). Here we make use of one of these parametrizations to illustrate how one may compute the evolution of porosity and density profiles in a sediment column.

We adopt a parametrization in which porosity changes at a rate that depends on the porosity itself and the difference between lithostatic pressure and hydrostatic pressure, $\sigma(z) = P_{\text{lithostatic}}(z) - P_{\text{hydrostatic}}(z)$ (eq. 16; Villa 2010). To obtain expressions for $P_{\text{lithostatic}}(z)$ and $P_{\text{hydrostatic}}(z)$, we apply the same simplification adopted in deriving eqs (9)–(13); that is, the pore space is fully saturated in marine settings and fully dry in terrestrial settings. This yields $P_{\text{hydrostatic}}(z) = \rho_w g S + \rho_w C g z$, and $P_{\text{lithostatic}}(z) = \rho_w g S + \int_0^z [\rho_s - (\rho_s - \rho_w C)\phi] g \, \mathrm{d}z'$, where z' is a variable of integration from the top of the sediment column ($z' = 0$) downward to $z' = z$. $P_{\text{hydrostatic}}(z)$ is zero on land since both the ocean function C and the ocean thickness S are zero over continents. Under the assumption that ρ_s, ρ_w and g remain constant with depth, we write

$$\begin{aligned}\frac{\mathrm{d}\phi}{\mathrm{d}t} &= -k\sigma(\phi - \phi_{\min}) \\ &= -kg\left\{\int_0^z [\rho_s - (\rho_s - \rho_w C)\phi]\,\mathrm{d}z' - \rho_w C z\right\}(\phi - \phi_{\min}) \\ &= -kgz(\rho_s - \rho_w C)(1 - \bar{\phi}_z)(\phi - \phi_{\min}). \end{aligned} \quad (16)$$

Here k is a rate constant for changes in porosity [$\mathrm{Pa}^{-1}\ \mathrm{s}^{-1}$], $\phi_{\min}$ is a minimum allowable porosity set by the densest possible grain packing (e.g. Bahr *et al.* 2001) and $\bar{\phi}_z$ is the mean porosity in the column from the top of the column to depth z ($\bar{\phi}_z = z^{-1}\int_0^z \phi \mathrm{d}z'$). This formulation for compaction differs from that in Pico *et al.* (2016), who applied a steady-state exponential porosity profile to the sediment to infer the amount of compaction since MIS 3. Since that approach does not include information about the rate of change of porosity, it cannot be used to compute transient changes in porosity, and thus cannot be used to treat the general case of transiently compacting sediment. By contrast, the parametrization in eq. (16) generates finite compaction rates that are a function of the sediment's weight, and thus can be used to compute transient changes in porosity even in the absence of deposition. Solving eqs (14)–(16) yields the evolution of the porosity profile $\phi(z)$ and the sediment thickness H.

To illustrate how porosity profiles evolve under this parametrization, we apply eqs (14)–(16) to an idealized column of saturated submarine sediment (the ocean function $C = 1$ in eq. 16). Fig. 3 shows the development of the porosity profile in the sediment column over 100 000 yr. Here, sediment with a porosity $\phi_{\max} = 0.6$ is deposited at a constant rate and compacts no further than a minimum porosity $\phi_{\min} = 0.2$, consistent with observations of maximum and minimum porosities in columns of sandy sediment (e.g. Bahr *et al.* 2001). Sediment compacts at a rate governed by eqs (14)–(16) with compaction rate coefficient $k = 10^{-17}\ \mathrm{Pa}^{-1}\ \mathrm{s}^{-1}$, starting with an initial sediment thickness $H = 0$ m. Figs 3(a)–(c) show the evolution of the porosity profile under slow ($B = 0.1\ \mathrm{mm\ yr}^{-1}$), moderate ($B = 1\ \mathrm{mm\ yr}^{-1}$) and fast deposition ($B = 10\ \mathrm{mm\ yr}^{-1}$), respectively. The fastest deposition rates in these simulations are comparable to those in some of the world's largest fluvial deltas (e.g. the Indus delta; Ferrier *et al.* 2015). The value of the compaction rate coefficient k was chosen to yield compaction rates similar to those in natural deltas; the compaction rates of 0–4.9 $\mathrm{mm\ yr}^{-1}$ in these simulations (Figs 4d–f) are comparable to Holocene compaction rates in the Mississippi delta (0.3–5 $\mathrm{mm\ yr}^{-1}$; Törnqvist *et al.* 2008).

The results illustrate how the deposition rate and the compaction rate influence the scale and shape of the porosity profiles, and thus influence changes in sea level (eqs 5–8). For example, Figs 3(d)–(i) show the mean porosity and density in the sediment columns as a function of time for the three sedimentation rates considered in Figs 3(a)–(c). Under the fastest deposition rates considered here, the mean porosity drops by more than a factor of two over 100 kyr (Fig. 3f) while the mean density increases by ∼30 per cent.

The solid lines in Figs 4(a)–(c) repeat the 100 kyr simulations in Figs 3(a)–(c), while the dashed line in each frame shows the growth of the sedimentary column for the same deposition rate without compaction. Figs 4(d)–(f) show the difference between the solid and dashed lines in each frame, that is, the error introduced into estimates of ΔH that neglect compaction. This error is ∼25 per cent, ∼65 per cent and ∼90 per cent of the compacted sediment thickness for the simulations in order of increasing deposition rates. These errors are largest in Fig. 4(f) because faster deposition generates faster compaction, which generates sediment thicknesses that diverge more from those in uncompacted sediment.

4 SEA-LEVEL RESPONSES TO SEDIMENT REDISTRIBUTION WITH AND WITHOUT COMPACTION

Using eqs (9)–(16), we modified the numerical model of Dalca *et al.* (2013) to account for sediment compaction and the exchange of water between the oceans and sedimentary pore space. We ran the model under two idealized sediment transfer scenarios, one including compaction and the other neglecting compaction, to quantify how compaction impacts spatial patterns in sea-level change. In each simulation we used a spherically symmetric Earth model characterized by a radial viscosity profile known as VM2 and an elastic lithosphere 90 km thick (Peltier 2004), density and elasticity profiles given by the Preliminary Reference Earth Model (PREM; Dziewonski & Anderson 1981), and modern topographic data from ETOPO2 (United States Department of Commerce 2001). Viscoelastic deformation in the sea-level response is modelled using Love number theory (Kendall *et al.* 2005) using both a full normal mode approach (Peltier 1985) and a collocation procedure (Mitrovica & Peltier 1992). We note that other approaches exist for computing solid Earth deformation that are based on Laplace-domain contour integration (e.g. Cambiotti & Sabadini 2010) or time domain forms of the governing equations (Latychev *et al.* 2005).

Modelled palaeo-sea-level histories are sensitive to uncertainties in the viscoelastic Earth parameters, an issue that has received considerable attention within the literature of glacial isostatic adjustment (e.g. Mitrovica & Milne 2002; Milne & Mitrovica 2008; Lambeck *et al.* 2014). Milne & Mitrovica (2008), for example, estimated that plausible uncertainties in the viscoelastic Earth parameters can lead to uncertainties of 15–20 m in model predictions of sea level at the Last Glacial Maximum at five sites with long observational records of palaeo-sea level (Barbados, Bonaparte Gulf, Huon Peninsula, Sunda Shelf and Tahiti). The following model results should therefore be considered as an illustrative example of the effects of compaction on sea level under a given set of Earth model parameters.

4.1 Model input: an idealized sediment transfer scenario

To begin, consider an idealized sediment transfer history for the Amazon River basin and its marine depositional fan (Fig. 5). This

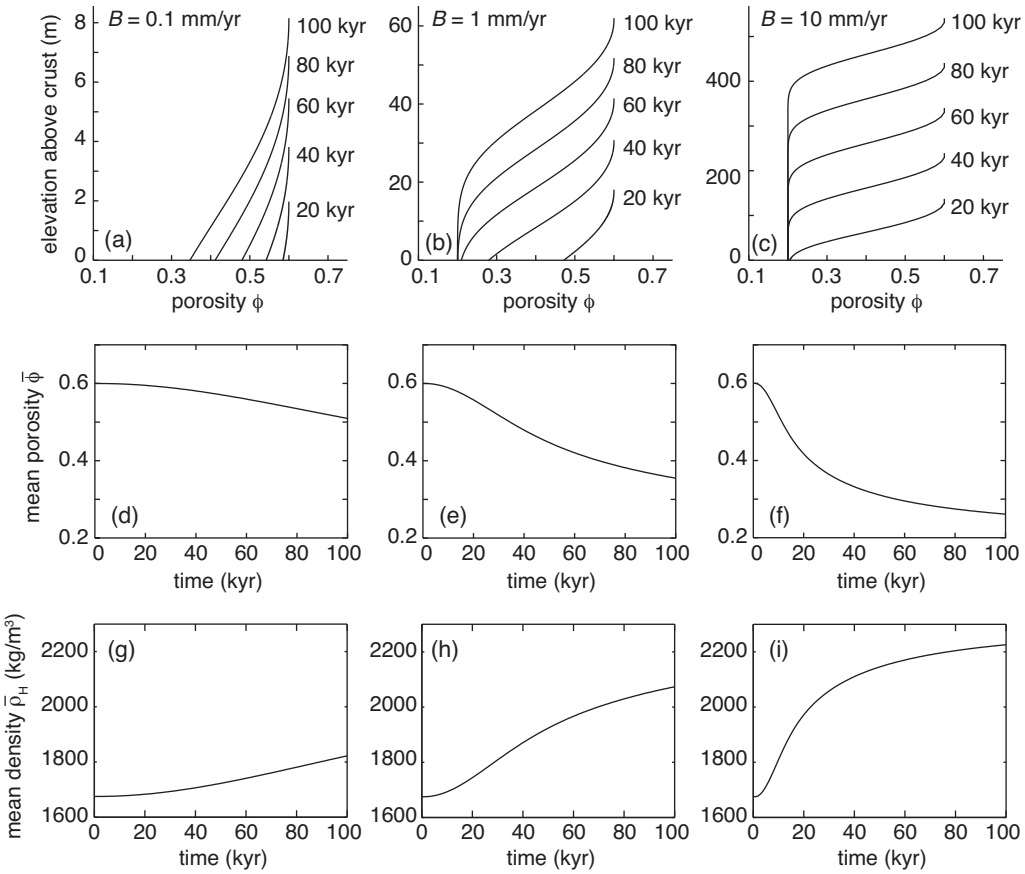

Figure 3. Sediment porosity profiles calculated with eqs (14)–(16) under steady deposition starting from zero sediment thickness, for deposition rates of $B = 0.1$ mm yr^{-1} (a), 1 mm yr^{-1} (b) and 10 mm yr^{-1} (c). Note differences in vertical scale among panels. (d–f) Mean sediment porosity during the simulations in panels (a)–(c), respectively. (g–i) Mean sediment density during the simulations in panels (a)–(c), respectively. Parameter values used in these simulations: $g = 9.8$ m s^{-2}; $\rho_s = 2650$ kg m^{-3}; $\rho_w = 1025$ kg m^{-3}; $\phi_{\min} = 0.2$; $\phi_{\max} = 0.6$; $k = 10^{-17}$ Pa^{-1} s^{-1}.

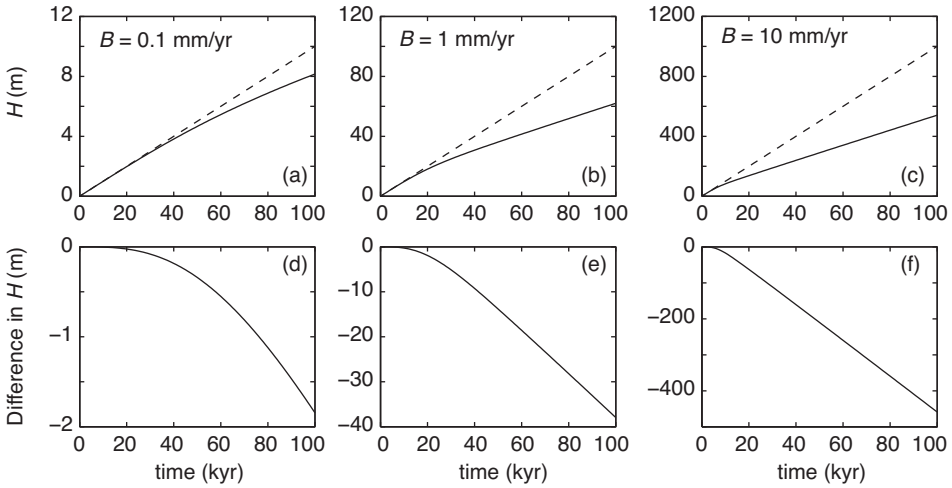

Figure 4. Evolution of the thickness of a saturated column of sediment under steady deposition. (a–c) Sediment thickness H at deposition rates of $B = 0.1$, 1 and 10 mm yr^{-1}, respectively. Solid lines indicate sediment thickness calculated with compaction ($k = 10^{-17}$ Pa^{-1} s^{-1}), under the same conditions as Fig. 3. Dashed lines indicate sediment thickness with no compaction ($k = 0$ Pa^{-1} s^{-1}). (d) Difference in sediment thickness between models with and without compaction in panel (a). Slope indicates rate of compaction. (e,f) As in panel (d), but for panels (b) and (c), respectively. Note differences in vertical scale among panels. Parameter values used in these simulations: $g = 9.8$ m s^{-2}; $\rho_s = 2650$ kg m^{-3}; $\rho_w = 1025$ kg m^{-3}; $\phi_{\min} = 0.2$; $\phi_{\max} = 0.6$.

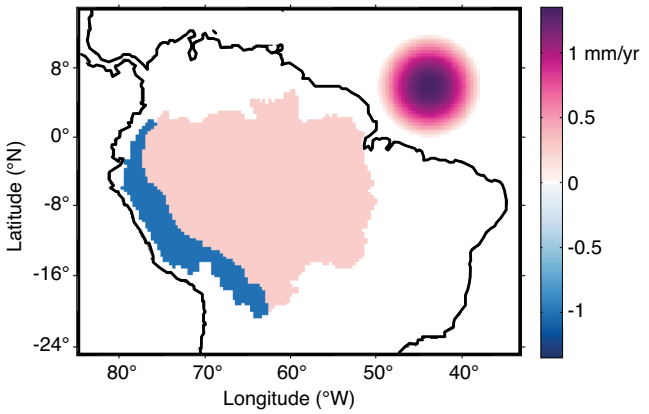

Figure 5. Deposition rates (positive; red) and erosion rates (negative; blue) used to create a synthetic sediment transfer scenario for the Amazon basin.

scenario is not intended to simulate sediment dynamics in the Amazon River system in detail; rather, our goal is to explore sea-level responses to sediment compaction under a few simple erosion and deposition conditions, albeit within a system with bulk continent-to-ocean sediment fluxes that are comparable to those in large river systems. To this end, we constructed the sediment transfer scenario with three different end-member environments: a depositional environment with saturated sediment, a depositional environment with dry sediment and an eroding environment with negligible porosity (Table 1).

To explore these three conditions, we divided the study area into three regions (Fig. 5). The first region spans the Andean highlands in the western part of the Amazon basin. We assigned this region a spatially uniform erosion rate of 1 mm yr^{-1}, comparable to Andean erosion rates determined from cosmogenic nuclide concentrations in detrital sediment (e.g. Safran *et al.* 2005; Wittmann *et al.* 2015). We assigned the eroding material a porosity $\phi = 0$, so that this region is representative of a material with the smallest possible porosity.

The second region consists of a marine depositional fan, which we modelled with a parabolic vertical cross section and a circular base of radius 6° centred at 6°N, 44°W. Deposition rates within it are scaled such that the integrated mass deposition rate is 1 Gt yr^{-1}, comparable to the 1.2 Gt yr^{-1} sediment flux of the Amazon River, which has the highest fluvial sediment flux on Earth (Milliman & Farnsworth 2011). This yielded a maximum deposition rate of 1.34 mm yr^{-1} at the centre of the deposit.

The third region spans the part of the Amazon basin outside the Andean highlands, and we refer to it here as the lowland region. We assigned the lowlands a spatially constant deposition rate of 0.28 mm yr^{-1}, calculated as the mass flux deposited on the lowlands (1.55 Gt yr^{-1}, the difference between the erosional mass flux from the highlands, 2.55 Gt yr^{-1}, and the deposited mass flux in the marine fan, 1 Gt yr^{-1}) divided by the area of the lowlands (5.28×10^6 km^2) and the initial density of the freshly deposited material (1060 kg m^{-3}, calculated as $\rho_s(1 - \phi_{\min})$). Sediment compaction in this subaerial region is parametrized in the same manner as it is in the submarine sediment. We follow the treatment in Section 2.3 in adopting the assumption that terrestrial sediment is dry, and note that simulations that include partial degrees of saturation can do so by using eqs (4)–(8) instead of eqs (9)–(13).

We used the rates in Fig. 5 to generate a sediment transfer history from 122 ka to the present. In this scenario (which we refer to as Scenario A), erosion rates and deposition rates remain constant over time, and vary in space according to the pattern in Fig. 5. Compaction of deposited sediment was computed following eqs (14)–(16).

We then generated a second sediment transfer scenario (Scenario B) using the same erosion and deposition rates in Fig. 5, but without compaction, which was accomplished by setting $k = 0$ in eq. (16). We then computed sea-level responses to each sediment transfer scenario. In both simulations, we maintained an unchanging global ice load with its modern-day distribution to isolate the impact of sediment redistribution on sea level.

4.2 Model output: changes in sea level, sediment thickness, crustal elevation and sea-surface equipotential

Fig. 6 summarizes the modelled sea-level responses to Scenarios A and B. Since these simulations do not include ice mass variations, changes in sea level result only from changes in ΔG, ΔR and ΔH (eq. 2). The top row of Fig. 6 shows the inputs and responses to Scenario A, which includes compaction, at the end of the 122 kyr simulation. Fig. 6(a) shows the sea-level changes ΔSL that result from the changes in sediment thickness ΔH (Fig. 6b). Fig. 6(c) shows the component of ΔSL due to changes in crustal elevation, ΔR. Perturbations in the gravity field ΔG (not shown) are as large as 0.9 m and are much smaller than the other components affecting ΔSL (e.g. ΔG is only ∼1 per cent of ΔR in the same location). The second row of Fig. 6 is analogous to the first row, but it shows inputs and responses for Scenario B, which neglects compaction. The third row shows the differences in the results in the first two rows. We stress that these simulations do not include ice mass variations, which are the dominant driver of sea-level change over glacial-interglacial timescales, and therefore are not meant to simulate the actual history of regional sea-level change in the Amazon system. Rather, they are intended to isolate the effects of compaction on changes in sea level under a simplified sediment transfer scenario.

4.3 Implications of sediment compaction for modelling sea-level change

A comparison of Figs 6(a)–(c) indicates that changes in sea level are dominated by changes in the sediment thickness ΔH and radial displacement of the crust, ΔR. In the centre of the marine fan,

Table 1. Erosion and deposition rates (B), sediment porosity (ϕ) and mean sediment density ($\bar{\rho}_H$) in sediment transfer scenarios. Negative B values indicate erosion.

	Marine fan	Highlands	Lowlands
Area (km^2)	1.40×10^6	9.64×10^5	5.28×10^6
Deposition rate B (mm yr^{-1})	Spatially variable	-1	0.28
Porosity ϕ at surface	$\phi_{\max}$	0	$\phi_{\max}$
Porosity ϕ at depth (Scenario A)	$\phi_{\min} < \phi < \phi_{\max}$	0	$\phi_{\min} < \phi < \phi_{\max}$
Porosity ϕ at depth (Scenario B)	$\phi_{\max}$	0	$\phi_{\max}$
Mean density $\bar{\rho}_H$	$\rho_s - (\rho_s - \rho_w)\bar{\phi}$	ρ_s	$\rho_s(1 - \bar{\phi})$

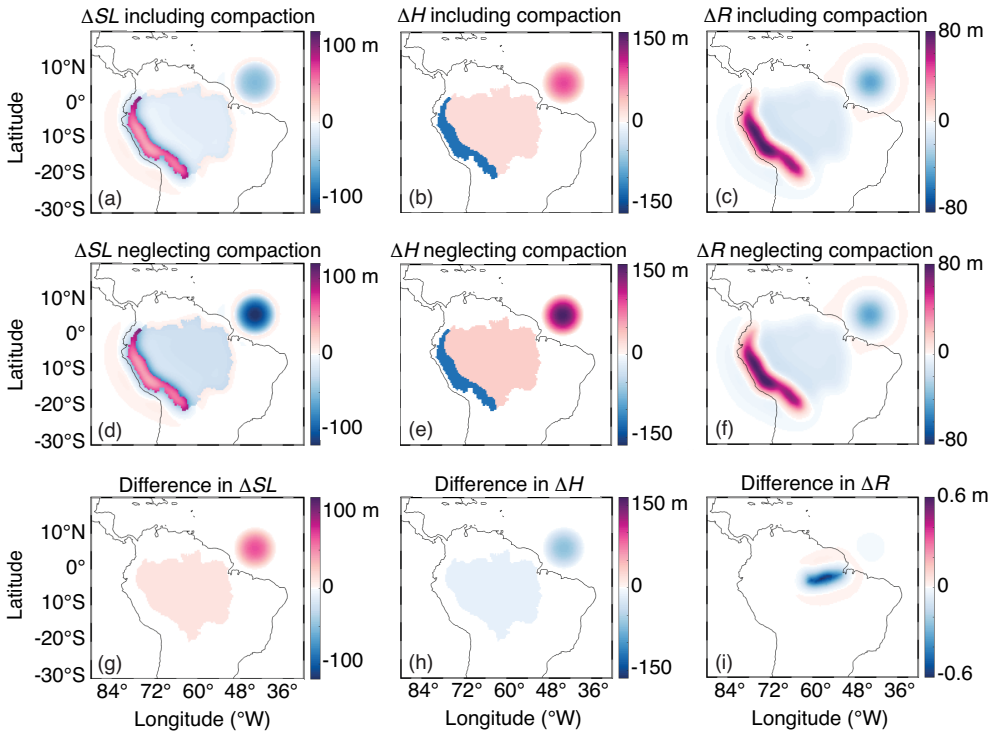

Figure 6. (a) Changes in sea level ΔSL over one 122 kyr simulation under sediment transfer Scenario A, which includes sediment compaction. (b,c) Changes in input sediment thickness ΔH and computed crustal elevation ΔR, respectively, at the end of the same simulation. (d–f) As in panels (a–c), but for Scenario B, which neglects compaction. (g) Difference in ΔSL between Scenarios A and B (panel a minus panel d) isolates the effect of compaction on ΔSL. (h,i) As in panel (g), but for ΔH and ΔR, respectively. Parameter values used in these simulations: $g = 9.81$ m s^{-2}; $\rho_s = 2650$ kg m^{-3}; $\rho_w = 1000$ kg m^{-3}; $\phi_{min} = 0.2$; $\phi_{max} = 0.6$; $k = 10^{-17}$ Pa^{-1} s^{-1}.

$\Delta H = 96.5$ m and $\Delta R = -43.4$ m, which, when input into eq. (2), combine to account for >99 per cent of the cumulative change in sea level ΔSL. Changes in the elevation of the sea-surface equipotential ΔG are therefore negligible in this scenario. In Scenario B, in which compaction is neglected (Figs 6d–f), ΔH and ΔR dominate ΔSL in the same manner. These results are consistent with modelled sea-level responses to more detailed histories of sediment redistribution in the Indus River-Arabian Sea system, in which ΔH and ΔR also dominate ΔSL (Ferrier *et al.* 2015).

A comparison of Figs 6(g)–(i) indicates that errors in ΔSL introduced by neglecting compaction are dominated by the direct effect of compaction on changes in sediment thickness ΔH. The effects of compaction on predictions on ΔR are significantly smaller (Fig. 6i). The largest effects of compaction on ΔR are localized to a corridor along the lowest lying reach of the Amazon River, where they peak at a maximum magnitude of 0.6 m, or 5 per cent of the effect of compaction on ΔSL in the same location (Fig. 6g). These small differences in ΔR between Scenarios A and B are produced as a result of differences in the sediment thickness history, which affects the history of shoreline migration and therefore water loading. That is, differences in ΔR between Scenarios A and B occur because this region was flooded by seawater to a greater extent in Scenario B than in Scenario A at the onset of the simulations. Over the course of the simulations, this region experienced a larger loss of water load—and thus a larger positive component of ΔR due to changes in water loading—in Scenario B than in Scenario A. These results highlight the relatively minor effect compaction can have on crustal elevation in places where the compaction affects the history of water loading, and also that those effects are dwarfed by compaction's direct effect on ΔH.

Fig. 6(g) shows that the impact of sediment compaction on ΔSL is greatest where compaction is fastest, which in this simulation is in the centre of the marine fan. Neglecting compaction in the fan leads to errors as large as ∼68 m at the centre of the fan by the end of the 122 kyr simulation, which is ∼40 per cent of the ΔSL that would occur there in the absence of compaction (Fig. 6d). Fig. 6(g) also shows that compaction affects predictions of ΔSL by as much ∼13 m in the lowlands, or ∼40 per cent of the ΔSL that would occur there in the absence of compaction. The differences in ΔSL in the lowlands are almost entirely due to the direct effect of sediment compaction. This is reflected in the relative magnitudes of the differences in ΔH and ΔR in Figs 6(h) and (i), which show that the difference in ΔH in this region is ∼12 m, or at least 20 times larger than the differences in ΔR, which reach a maximum value of ∼0.6 m in the same region.

The central implication of these results is that compaction can have significant effects on ΔSL over ∼100 kyr timescales, and that the impact of compaction on sea level is dominated by its direct effect on the elevation of the solid surface. Under the sediment transfer scenario applied here, neglecting compaction can lead to errors in ΔSL of several tens of per cent in the areas undergoing the fastest deposition.

5 CONCLUSIONS

We have provided a method for incorporating sediment redistribution and compaction into gravitationally self-consistent ice age sea-level theory. Applying this method requires the calculation of two additional quantities—the mean porosity in the sediment column,

and the degree of saturation in the sediment column—that were not accounted for in previous treatments of ice age sea-level change in the presence of sediment redistribution (Dalca *et al.* 2013). One of the advantages of our method for computing sea-level changes is its flexibility, which permits the user to adopt any model for compaction, provided that the compaction model can be used to compute the mean sediment porosity and degree of saturation. This may be particularly valuable for refining sea-level histories for periods when sea level was much lower than it is today (e.g. Hanebuth *et al.* 2006; Simms *et al.* 2009; Pico *et al.* 2016), which tend to have fewer empirical constraints on palaeo-sea-level history because palaeo-sea-level markers from these periods are presently submarine, and hence have been more difficult to access than palaeo-sea-level markers that are currently subaerial.

To illustrate the model's utility, we computed sedimentary responses to deposition and compaction under an adopted parametrization for the rate of change of porosity. We used this parametrization to compute sea-level responses to an idealized history of sediment erosion and deposition for the Amazon basin and offshore fan over a 122-kyr ice age cycle. The model results show that compaction can strongly influence changes in sea level, especially in areas of relatively rapid deposition. This influence is dominated by the direct effect of compaction on sediment thickness, while changes in crustal elevation and sea-surface equipotential are much smaller contributors to the computed change in sea level. These simulations lay the foundation for modelling sea-level responses to more detailed sediment transfer and compaction scenarios. In doing so, this work provides a more refined tool for interpreting palaeoclimatic and tectonic influences on past sea-level changes.

ACKNOWLEDGEMENTS

We thank Torbjörn Törnqvist, one anonymous reviewer and the Editor for insightful comments that significantly improved this manuscript. This study was supported by National Science Foundation grant EAR-1525922 to KLF and JXM and by an NSF Graduate Research Fellowship to TP.

REFERENCES

Audet, D.M. & Fowler, A.C., 1992. A mathematical model for compaction in sedimentary basins, *Geophys. J. Int.,* **110,** 577–590.

Austermann, J. & Mitrovica, J.X., 2015. Calculating gravitationally self-consistent sea level changes drives by dynamic topography, *Geophys. J. Int.,* **203,** 1909–1922.

Bahr, D.B., Hutton, E.W.H., Syvitski, J.P.M. & Pratson, L.F., 2001. Exponential approximations to compacted sediment porosity profiles, *Comput. Geosci.,* **27,** 691–700.

Bindlish, R., Jackson, T., Cosh, M., Zhao, T. & O'Neill, P., 2015. Global soil moisture from the Aquarius/SAC-D satellite: Description and initial assessment, *IEEE Geosci. Remote Sens. Lett.,* **12,** 923–927.

Biot, M.A., 1941. General theory of three-dimensional consolidation, *J. Appl. Phys.,* **12,** 155–164.

Bloom, A.L., 1964. Peat accumulation and compaction in a Connecticut coastal marsh, *J. Sedimentary Petrol.,* **34,** 599–603.

Blum, M.D. & Roberts, H.H., 2009. Drowning of the Mississippi Delta due to insufficient sediment supply and global sea-level rise, *Nat. Geosci.,* **2,** 488–491.

Brain, M.J., Long, A.J., Woodroffe, S.A., Petley, D.N., Milledge, D.G. & Parnell, A.C., 2012. Modelling the effects of sediment compaction on salt marsh reconstructions of recent sea-level rise, *Earth planet. Sci. Lett.,* **345–348,** 180–193.

Brain, M.J., Kemp, A.C., Horton, B.P., Culver, S.J., Parnell, A.C. & Cahill, N., 2015. Quantifying the contribution of sediment compaction to late Holocene salt-marsh sea-level reconstructions, North Carolina, USA, *Quat. Res.,* **83,** 41–51.

Cambiotti, G. & Sabadini, R., 2010. The compressional and compositional stratifications in Maxwell earth models: the gravitational overturning and the long-period tangential flux, *Geophys. J. Int.,* **180,** 475–500.

Chappell, J., 1974. Geology of coral terraces, Huon Peninsula, New Guinea: a study of Quaternary tectonic movements and sea-level changes, *Bull. geol. Soc. Am.,* **85,** 553–570.

Church, J.A. *et al*., 2013. Sea Level Change, in *Climate Change 2013: The Physical Science Basis. Contribution of Working Group I to the Fifth Assessment Report of the Intergovernmental Panel on Climate Change*, pp. 1137–1216, eds Stocker, T.F., Qin, D., Plattner, G.-K., Tignor, M., Allen, S.K., Boschung, J., Nauels, A., Xia, Y., Bex, V. & Midgley, P.M., Cambridge Univ. Press.

Dalca, A.V., Ferrier, K.L., Mitrovica, J.X., Perron, J.T. & Milne, G.A., 2013. On postglacial sea level – III. Incorporating sediment redistribution, *Geophys. J. Int.,* **194,** 45–60.

d'Alpoim Guedes, J., Austermann, J. & Mitrovica, J.X., 2016. Lost foraging opportunities for east Asian hunter-gatherers due to rising sea level since the last glacial maximum, *Geoarchaeology,* **31,** 255–266.

Dziewonski, A.M. & Anderson, D.L., 1981. Preliminary reference Earth model, *Phys. Earth planet. Inter.,* **25,** 297–356.

Edwards, R.J., 2006. Mid- to late-Holocene relative sea-level change in southwest Britain and the influence of sediment compaction, *Holocene,* **16,** 575–587.

Farrell, W.E. & Clark, J.A., 1976. On postglacial sea level, *Geophys. J. R. astr. Soc.,* **47,** 647–667.

Ferrier, K.L., Mitrovica, J.X., Giosan, L. & Clift, P.D., 2015. Sea-level responses to erosion and deposition of sediment in the Indus River basin and the Arabian Sea, *Earth planet. Sci. Lett.,* **416,** 12–20.

Gibson, R.E., England, G.L. & Hussey, M.J.L., 1967. The theory of one-dimensional consolidation of saturated clays, *Geotechnique,* **17,** 261–273.

Gibson, R.E., Schiffman, R.L. & Cargill, K.W., 1981. The theory of one-dimensional consolidation of saturated clays. II. Finite nonlinear consolidation of thick homogeneous layers, *Can. Geotech. J.,* **18,** 280–293.

Hanebuth, T.J.J., Saito, Y., Tanabe, S., Vu, Q.L. & Ngo, Q.T., 2006. Sea levels during late marine isotope stage 3 (or older?) reported from the Red River delta (northern Vietnam) and adjacent regions, *Quat. Int.,* **145–146,** 119–134.

Hay, C.C., Morrow, E., Kopp, R.E. & Mitrovica, J.X., 2015. Probabilistic reanalysis of twentieth-century sea-level rise, *Nature,* **517,** 481–484.

Horton, B.P. & Shennan, I., 2009. Compaction of Holocene strata and the implications for relative sea-level change on the east coast of England, *Geology,* **37,** 1083–1086.

Horton, B., Engelhart, S.E., Hill, D.F., Kemp, A.C., Nikitina, D.L., Miller, K.G. & Peltier, W.R., 2013. Influence of tidal-range change and sediment compaction on Holocene relative sea-level change in New Jersey, USA, *J. Quat. Sci.,* **28,** 403–411.

Johnston, P., 1993. The effect of spatially non-uniform water loads on predictions of sea level change, *Geophys. J. Int.,* **114,** 615–634.

Kaye, C.A. & Barghoorn, E.S., 1964. Late quaternary sea-level change and crustal rise at Boston, Massachusetts, with notes on the autocompaction of peat, *Bull. geol. Soc. Am.,* **75,** 63–80.

Kendall, R.A., Mitrovica, J.X. & Milne, G.A., 2005. On post-glacial sea level – II. Numerical formulation and comparative results on spherically symmetric models, *Geophys. J. Int.,* **161,** 679–706.

Khan, S.R. & Islam, M.B., 2008. Holocene stratigraphy of the lower Ganges-Brahmaputra river delta in Bangladesh, *Frontiers Earth Sci. China,* **2,** 393–399.

Kuehl, S.A., Levy, B.M., Moore, W.S. & Allison, M.A., 1997. Subaqueous delta of the Ganges-Brahmaputra river system, *Mar. Geol.,* **144,** 81–96.

Lambeck, K., Purcell, A., Johnston, P., Nakada, M. & Yokoyama, Y., 2003. Water-load definition in the glacio-hydro-isostatic sea-level equation, *Quat. Sci. Rev.,* **21,** 309–318.

Lambeck, K., Rouby, H., Purcell, A., Sun, Y. & Sambridge, M., 2014. Sea level and global ice volumes from the Last Glacial Maximum to the Holocene, *Proc. Natl. Acad. Sci. USA,* **111**(43), 15 296–15 303.

Latychev, K., Mitrovica, J.X., Tromp, J., Tamisiea, M.E., Komatitsch, D. & Christara, C.C., 2005. Glacial isostatic adjustment on 3-D Earth models: a finite volume formulation, *Geophys. J. Int.,* **161,** 421–444.

Martinec, Z., 2000. Spectral–finite element approach to three-dimensional viscoelastic relaxation in a spherical earth, *Geophys. J. Int.,* **142,** 117–141.

Michels, K.H., Suckow, A., Breitzke, M., Kudrass, H.R. & Kottke, B., 2003. Sediment transport in the shelf canyon "Swatch of No Ground" (Bay of Bengal), *Deep-Sea Res. II,* **50,** 1003–1022

Milliman, J.D. & Farnsworth, K.L., 2011. *River Discharge to the Coastal Ocean,* Cambridge Univ. Press, 392 pp.

Milne, G.A., 1998. Refining models of the glacial isostatic adjustment process, *PhD thesis*, University of Toronto, Toronto.

Milne, G.A. & Mitrovica, J.X., 1996. Postglacial sea-level change on a rotating Earth: first results from a gravitationally self-consistent sea-level equation, *Geophys. J. Int.,* **126,** F13–F20.

Milne, G.A. & Mitrovica, J.X., 1998. Postglacial sea-level change on a rotating Earth, *Geophys. J. Int.,* **133,** 1–19.

Milne, G.A. & Mitrovica, J.X., 2008. Searching for ecstasy in deglacial sea-level histories, *Quat. Sci. Rev.,* **27,** 2292–2302.

Milne, G.A., Mitrovica, J.X. & Davis, J.L., 1999. Near-field hydro-isostasy: the implementation of a revised sea-level equation, *Geophys. J. Int.,* **139,** 464–482.

Mitrovica, J.X. & Milne, G.A., 2002. On the origin of postglacial ocean syphoning, *Quat. Sci. Rev.,* **21,** 2179–2190.

Mitrovica, J.X. & Peltier, W.R., 1992. A comparison of methods for the inversion of viscoelastic relaxation spectra, *Geophys. J. Int.,* **108,** 410–414.

Munk, W.H. & Macdonald, G.J.F., 1960. *The Rotation of the Earth,* Cambridge Univ. Press.

Paul, M.A. & Barras, B.F., 1998. A Geotechnical correction for post-depositional sediment compression: examples from the Forth valley, Scotland, *J. Quat. Sci.,* **13,** 171–176.

Peltier, W.R., 1985. The LAGEOS constraint on deep mantle viscosity: results from a new normal mode method for the inversion of viscoelastic relaxation spectra, *J. geophys. Res.,* **90,** 9411–9421.

Peltier, W.R., 1994. Ice age paleotopography, *Science,* **265,** 195–201.

Peltier, W.R., 1998. 'Implicit ice' in the global theory of glacial isostatic adjustment, *Geophys. Res. Lett.,* **25,** 3955–3958.

Peltier, W.R., 2004. Global glacial isostasy and the surface of the ice-age Earth: the ICE-5 G (VM2) model and GRACE, *Annu. Rev. Earth Planet. Sci.,* **32,** 111–149.

Pico, T., Mitrovica, J.X., Ferrier, K.L. & Braun, J., 2016. Global ice volume during MIS 3 inferred from a sea-level analysis of sedimentary core records in the Yellow River Delta, *Quat. Sci. Rev.,* **152,** 72–79.

Pizzuto, J.E. & Schwendt, A.E., 1997. Mathematical modeling of auto-compaction of a Holocene transgressive valley-fill deposit, Wolfe Glade, Delaware, *Geology,* **25,** 57–60.

Safran, E.B., Bierman, P.R., Aalto, R., Dunne, T., Whipple, K.X. & Caffee, M., 2005. Erosion rates driven by channel network incision in the Bolivian Andes, *Earth Surf. Process. Landf.,* **30,** 1007–1024.

Simms, A.R., DeWitt, R., Rodriguez, A.B., Lambeck, K. & Anderson, J.B., 2009. Revisiting marine isotope stage 3 and 5a (MIS3-5a) sea levels within the northwestern Gulf of Mexico, *Glob. Planet. Change,* **66,** 100–111.

Teatini, P., Tosi, L. & Strozzi, T., 2011. Quantitative evidence that compaction of Holocene sediments drives the present land subsidence of the Po Delta, Italy, *J. geophys. Res.,* **116,** B08407, doi:10.1029/2010JB008122.

Törnqvist, T.E. *et al.*, 2008. Mississippi Delta subsidence primarily caused by compaction of Holocene strata, *Nat. Geosci.,* **1,** 173–176.

United States Department of Commerce National Oceanic and Atmospheric Administration National Geophysical Data Center, 2001. '2-Minute gridded global relief data (ETOPO2)'. Available at: http://www.ngdc.noaa.gov/mgg/fliers/01mgg04.html, last accessed January 2006.

Villa, A., 2010. *Three Dimensional Geophysical Modeling: from Physics to Numerical Simulation,* Ledizioni Ledi Publishing, Milan, Italy.

Wilson, C.A. & Goodbred, S.L., 2014. Construction and maintenance of the Ganges-Brahmaputra-Meghna delta: linking process, morphology, and stratigraphy, *Annu. Rev. Mar. Sci.,* **7,** 67–78.

Wittmann, H. *et al*., 2015. A test of the cosmogenic ^{10}Be(meteoric)/^{9}Be proxy for simultaneously determining basin-wide erosion rates, denudation rates, and the degree of weathering in the Amazon basin, *J. geophys. Res.,* **120,** 2498–2528.

Wolstencroft, M., Shen, Z., Törnqvist, T.E., Milne, G.A. & Kulp, M., 2014. Understanding subsidence in the Mississippi Delta region due to sediment, ice and ocean loading: insights from geophysical modeling, *J. geophys. Res.,* **119,** 3838–3856.

Wu, P. & van der Wal, W., 2003. Postglacial sea levels on a spherical, self-gravitating viscoelastic Earth: effects of lateral viscosity variations in the upper mantle on the inference of viscosity contrasts in the lower mantle, *Earth planet. Sci. Lett.,* **211,** 57–68.

Zhong, S., Paulson, A. & Wahr, J., 2003. Three-dimensional finite element modeling of Earth's viscoelastic deformation: effects of lateral variations in lithospheric thickness, *Geophys. J. Int.,* **155,** 679–695.